Molecular Crystals and Liquid Crystals

ISSN: 1542-1406 (Print) 1563-5287 (Online) Journal homepage: http://www.tandfonline.com/loi/gmcl20

# Modelling and diagnostic of an ultrasonic piezoelectric actuator

S. Latrèche, M. Mostefai, M. Meddad, A. Eddiai, B. Sahraoui, M. Khemliche & A. Badoud

**To cite this article:** S. Latrèche, M. Mostefai, M. Meddad, A. Eddiai, B. Sahraoui, M. Khemliche & A. Badoud (2016) Modelling and diagnostic of an ultrasonic piezoelectric actuator, Molecular Crystals and Liquid Crystals, 628:1, 23-40, DOI: 10.1080/15421406.2015.1137121

**To link to this article:** http://dx.doi.org/10.1080/15421406.2015.1137121

Published online: 13 May 2016.

MOL. CRYST. LIQ. CRYST.
2016, VOL. 628, 23–40
http://dx.doi.org/10.1080/15421406.2015.1137121

Taylor & Francis
Taylor & Francis Group

# Modelling and diagnostic of an ultrasonic piezoelectric actuator

S. Latrèche[a], M. Mostefai[a], M. Meddad[b], A. Eddiai[c], B. Sahraoui[d], M. Khemliche[a], and A. Badoud[a]

[a]Automatic Laboratory of Setif, Electrical Engineering Department, University of Setif, Algeria; [b]DAC HR Laboratory Sétif, University Mohamed el Bachir el Ibrahimi BBA, Algeria; [c]Laboratoire de physique de la matière condensée, Faculté des Sciences Ben M'sik, Université Hassan II, Casablanca, Morocco; [d]LUNAM Université, Université d'Angers, Laboratoire MOLTECH-Anjou, ANGERS Cedex, France

**ABSTRACT**
Modeling of piezoelectric motors is a difficult task because their characteristics are affected by various factors such as materials properties, electrical and mechanical boundary conditions. This work presents the modeling of piezoelectric motor via bond graph method and used for the diagnostic. This method is an innovative way to analyse the effects of different design variables on the objective function but can be also considered as an optimization stage of the study. The validation and the development of bond graph models are based on physical insight to aid in structural damage detection and use the technique of optimal sensors placement.

**KEYWORDS**
Modeling; Diagnostic; Ultrasonic Linear Motor; Piezoelectric Actuator; Bond Graph

## 1. Introduction

In recent years industry has shown growing interest in linear ultrasonic piezoelectric actuators and ultrasonic drives. The piezoelectric actuators make possible the systems which are with simple design and are finding wider application in positioning systems. There are growing demands for actuators with a volume of less than 1 $mm^3$. This need has been reported across the micro-robotics industry [1] and the medical profession [2, 3].

The description of piezoactuator involves combined mechanical and electrical effects. Often the operating conditions are chosen to achieve a nearly linear behaviour [4]. Therefore, we focus on modeling the structural dynamics of the piezoactuator.

The modeling constitutes an aspect of great importance within all engineering fields because it allows us to understand the behaviour of the system without having to experiment on it. It also allows the determination of certain characteristics of the system and can give important information on operating conditions with the use of relatively simple and inexpensive procedures. Moreover, it is an essential tool for the design of fault detection and isolation strategies and very important at industrial level [5].

In literature, three different modeling approaches are used to describe the behaviour of the piezoactuators; bending beam analogies, thermal analogies and energy approaches. A model incorporating hysteresis is derived using beam analogy in [6] for a three layer bimorph beam

**CONTACT** S. Latrèche ksamia2002@yahoo.fr Automatic Laboratory of Setif, Electrical Engineering Department, University of Setif, Algeria
Color versions of one or more of the figures in the article can be found online at www.tandfonline.com/gmcl.

consisting of two piezoelements separated by a metal shim. Thermal analogy methods are based on the similarities between the piezostrains and thermal strains [7, 8, 9].

The electromechanical coupling of piezoactuators can be modelled using energy based methods [10]. The dynamics of single stacked piezoactuators are described using electromechanical models in [11, 12, 13]. The different layers of a piezostack can be modelled as a chain of lumped mass-spring-damper systems, where also the nonlinear hysteresis effects are incorporated into the model.

Fault detection and isolation in complex dynamic systems requires the use of the modeling approaches that capture system dynamics and the transients that arise when faults occur. In the previous work [5], we have developed a systematic approach using bond graph modeling to derive the temporal causal graph representing the functional relations of a system subject to FDI (Fault detection and isolation).

The inherent physical constraints of a bond graph model (conservation of energy, conservation of the physical state, continuity of power) result in well constrained models that prevent the generation of spurious results, one of the most important drawbacks of traditional qualitative methods used in artificial intelligence approaches to the diagnosis problem. The generation of the bond graph modeling approach, allows seamless integration of multi domain models (electrical, mechanical and hydraulic) into one representation.

The contributions of this paper are threefold. Firstly, a bond graph model of the ultrasonic actuator based on its physical properties is derived. Secondly, bond graph model with sensor placement are derived. Finally, the results are validated by software of simulation. From the model structure control, oriented models can be derived. Due to the energy based modeling approach, the model can be easily extended with the dynamics of the system to be actuated and with nonlinear effects, such as hysteresis, stick-slip, etc.

We also show how the qualitative approach to FDI, embodied by the transcend system applies to the fault isolation in the ultrasonic linear motor.

## 2. Graphical modeling using bond graph approach

Bond graph is an explicit graphical tool for capturing the structures among the physical systems and representing the mass an energy network based on the exchange of power [14]. Some authors [15, 16] have extended the bond graph concept to represent phenomena such as chemical kinetics and to extract causal models and control structures from the bond graph networks.

One of the advantages of bond graph method is that models of various systems belonging to different engineering domains can be expressed using a set of only nine elements: inertial elements (I), capacitive elements (C), resistive elements (R), effort sources (Se), flow sources (Sf), transformer elements (TF), gyrator elements (GY), 0–junctions (0-J) and 1– junctions (1-J). I, C, and R elements are passive elements that convert the supplied energy into stored or dissipated energy. Se and Sf elements are active elements supplying power to the system. TF, GY, 0-J and 1-J are junction elements that connect I, C, R, Se and Sf effectively creating the structure of the bond graph model [17, 18, 19].

Bond graph models are ideally suited for modeling a nonlinear system. A bond graph model does not assume any linearity constraints. The model hides the complexity of nonlinearity from the user of the model. Once the modeller defines the nonlinear relationship in the model, it is the job of the underlying bond graph software to solve the model. The whole process is transparent to the user of the model.

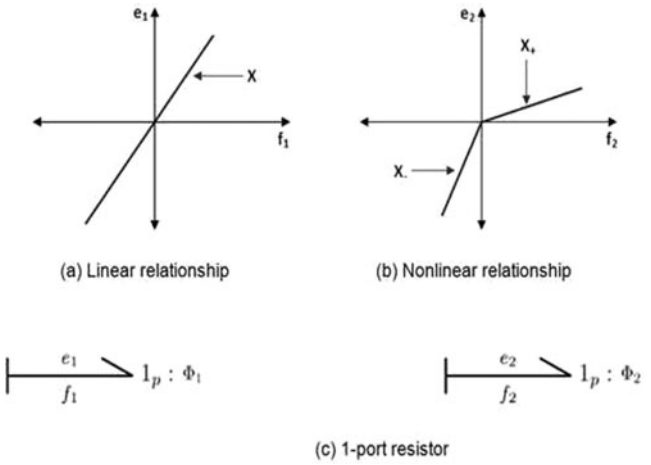


**Figure 1.** Relationship between flow and effort for 1-port resistor elements.

Bond graph models are ideally suited for modeling a nonlinear system. A bond graph model does not assume any linearity constraints. The model hides the complexity of nonlinearity from the users of the model. The modellers define the nonlinear relationship in the model. It is the job of the underlying bond graph software to solve the model. The whole process is transparent to the users of the model.

1-port element is the most basic of the bond graph elements. This element has a single port for energy exchange with its environment. There will be a constitutive equation depicting the relationship between the co-variables (effort and flow) of the bond.

The constraint on the constitutive equation is that the energy should be conserved as the underlying physical law of bond graph modeling. Two different relationships between the co-variables are depicted graphically in Figure (1–a) and (1–b). The bond graph model for this relationship is depicted by 1-port elements in Figure (1–c).

The constitutive relationship for the resistor elements are given in equations (1) and (2). It can be seen that the model for both linear and nonlinear behaviour look-alike, with the constitutive relationship hiding the difference. It is the job of the solver software to simulate the model differently.

$$e_1 = \varphi_1\left(f_1\right) \tag{1}$$

$$e_2 = \varphi_2\left(f_2\right) \tag{2}$$

$$\text{where, } \begin{cases} \phi_1 = X \ \text{ always} \\ \phi_2 = X_- \ \text{ if } f_2 < 0 \\ \phi_2 = X_+ \ \text{ if } f_2 > 0 \end{cases} \tag{3}$$

## 3. Description of an ultrasonic piezoelectric actuator

Generally, ultrasonic piezoelectric motors can be designed to use either traveling waves or standing waves to generate motion. Piezoelectric standing wave motors use a combination of flexural, torsional or longitudinal vibrations of a piezoelectric actuator. One vibration produces a normal force while the other generates motion that is perpendicular to the normal force. This combination creates a friction based driving force between stationary component, the vibrator, and the object to be moved the slider. On the other hand, in a piezoelectric traveling wave motor, traveling waves are generated and propagate in both directions.

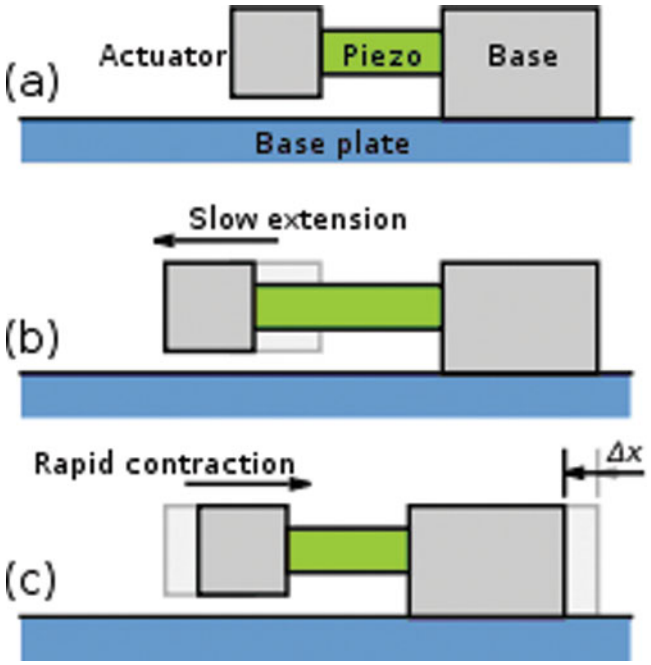


**Figure 2.** A direct drive mechanism of the actuator.

Such waves can be classified into two general types. The first type is known as Rayleigh wave [20]. An analogy of this kind of wave is the earthquakes. The other type of wave known as flexural wave propagates with a snake-like motion [21]. For both Rayleigh and flexural waves, a point on the surface will move following an elliptical trajectory. It is this elliptical

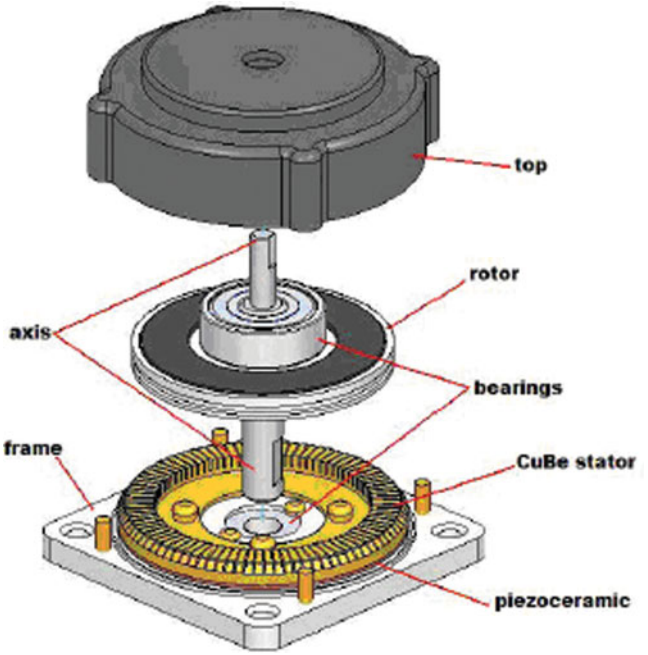


**Figure 3.** View of an ultrasonic piezoelctric motor.

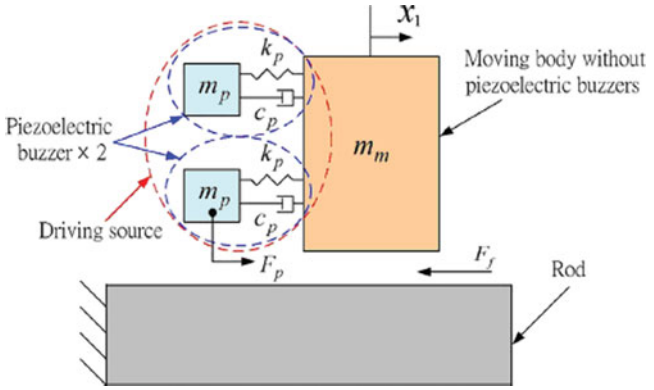


**Figure 4.** Mechanical model of the present piezoelectric actuator.

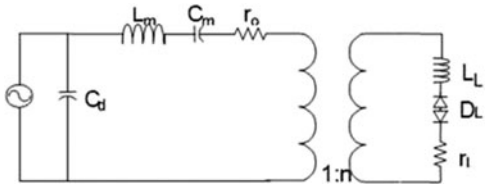


**Figure 5.** Single phase equivalent circuit for the motor.

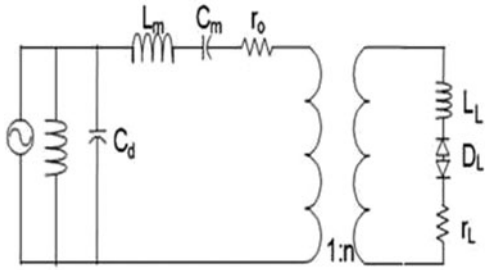


**Figure 6.** Canceling the effect of blocking capacitance.

motion that provides the drive in traveling wave motors. In the following sections, these two wave types are described more in details.

A mechanical wave is a disturbance which is created by a vibrating object and subsequently travels through a medium from one location to another, transporting energy as it moves [22]. The mechanism by which a mechanical wave propagates itself through a medium involves

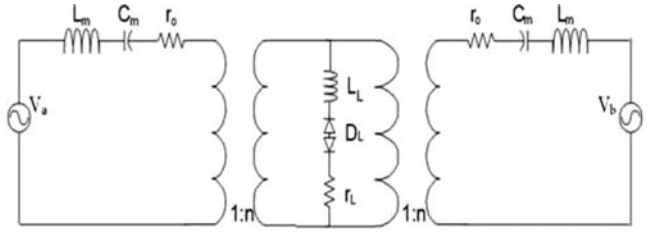


**Figure 7.** Equivalent electrical circuit of the complete motor.

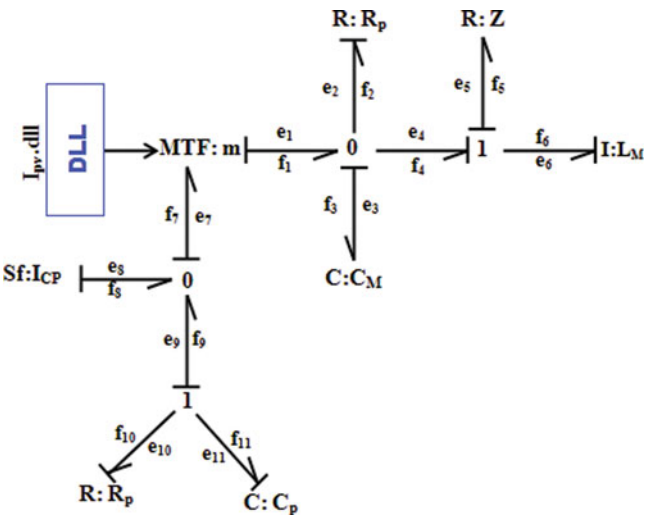


**Figure 8.** Bond Graph Model of stator with one excitation.

particle interaction; one particle applies a push or pull on its adjacent neighbour, causing a displacement of that neighbour from the equilibrium or rest position.

In one mechanism, the elongation in a single plane is used to make a series of stretches and position holds, similar to the way a caterpillar moves. Motors are made in both linear and rotary types. A technique is to use piezoelectric ceramics to push a stator. These piezoelectric motors use three groups of crystals: two of which are locking and one motive, permanently connected to either the motor's casing or stator (not both) and inserted between the other two, which provides the motion. These piezoelectric motors are fundamentally stepping motors, with each step comprising either two or three actions, based on the locking type. Another mechanism employs the use of surface acoustic waves (SAW) to generate linear or rotational motion.

A second drive technique is illustrated by the Squiggle motor, in which piezoelectric elements are bonded orthogonally to a nut and their ultrasonic vibrations rotate and translate a central lead screw. This is a direct drive mechanism.

We have decided to study the resonant annular piezomotor for different reasons: it has already proved his feasibility; it is the more efficient and have the highest torque actually. For the moment, it is the most advanced piezomotor.

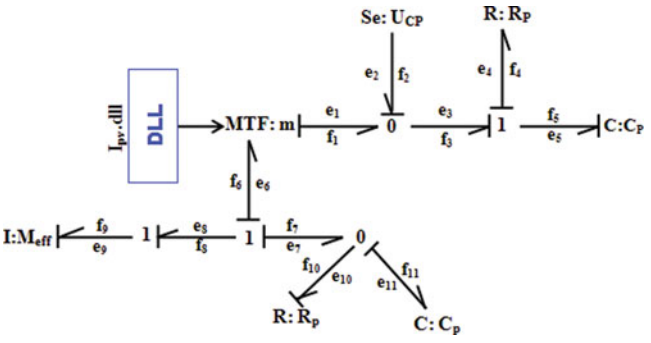


**Figure 9.** Bond Graph Model for the complete motor.

**Table 1.** Parameters of motor.

| Name | Symbol and value |
|---|---|
| Resistances of entries | Rp = 5Ω; Ds = 5Ω |
| Ceramics capacity | Cp = 7.8nF; 1/Cs = 7.87nF |
| Capacity of stator | CM = 0.42nF; Cp = 0.428nF |
| Effective mass | Meff = 40.5 Kg |
| Mass of rotor | M = (Meff+22.8+3) g |
| Distance stator's points | a = 4.5mm |
| Frequency of Resonance | wres2 = wres1<br>wres1 = 2∗pi∗43.365∗1kHz |
| Wavelength | λ = 2∗pi∗R w/n m |

**Table 2.** Table signature for [y1y2y3y4y5y6y7y8−×−1−×−2] = [0111111111].

| | I1 | I2 | R4 | R5 | R6 | r2 | I3 | I4 | C1 | C2 |
|---|---|---|---|---|---|---|---|---|---|---|
| ARR1 | 1 | 1 | 0 | 0 | 0 | 0 | 0 | 0 | 0 | 0 |
| ARR2 | 0 | 0 | 1 | 0 | 0 | 0 | 0 | 0 | 0 | 0 |
| ARR3 | 0 | 0 | 0 | 1 | 0 | 0 | 0 | 0 | 0 | 1 |
| ARR4 | 0 | 0 | 0 | 0 | 1 | 0 | 0 | 0 | 0 | 1 |
| ARR5 | 0 | 0 | 0 | 0 | 0 | 1 | 0 | 0 | 0 | 1 |
| ARR6 | 0 | 0 | 0 | 0 | 0 | 0 | 1 | 0 | 0 | 0 |
| ARR7 | 0 | 0 | 0 | 0 | 0 | 0 | 0 | 1 | 0 | 0 |
| ARR8 | 0 | 0 | 0 | 0 | 0 | 0 | 0 | 0 | 1 | 0 |
| ARR9 | 0 | 0 | 0 | 0 | 0 | 0 | 0 | 0 | 0 | 1 |

The operation principle is described on Figure 3. This motor is made of three main parts:

**Stator**: It is a beryllium-copper annular plate. At his circumference, teeth are machined to amplify the vibration movement and eliminate the wear particles. At its bottom surface, piezoelectric ceramics are glued to excite the metallic part. The stator is fixed to the frame at its center. To guarantee the free vibration of the stator ring, a decoupling fold is machined between the center and the circumference.

**Rotor**: It can be separated in 3 zones: The axis, output of the motor and the track friction in contact with the stator. The spring fold linking the axis to the track and giving the elasticity needed to apply rotor on stator.

**Stator/rotor interface**: The model of the interface stator-rotor is the most complex part in the ultrasonic motor model. It is supposed that the stator is rigid and its vibration profile does not change after the contact with the rotor, knowing that this one has a conform layer of contact. This part is the one where the interne functional behaviour is assured by the existence of some forces. These forces depend on comparison between the displacements speeds of the stator and the rotor respectively [23].

**Table 3.** Table signature For [y1y2y3y4y5y6y7y8−×−1−×−2−]− = [1111111110].

| | I1 | I2 | R4 | R5 | R6 | r2 | I3 | I4 | C1 | C2 |
|---|---|---|---|---|---|---|---|---|---|---|
| ARR1 | 1 | 0 | 0 | 0 | 0 | 0 | 0 | 0 | 0 | 0 |
| ARR2 | 0 | 1 | 0 | 0 | 0 | 0 | 0 | 0 | 0 | 0 |
| ARR3 | 0 | 0 | 1 | 0 | 0 | 0 | 0 | 0 | 0 | 1 |
| ARR4 | 0 | 0 | 0 | 1 | 0 | 0 | 0 | 0 | 0 | 1 |
| ARR5 | 0 | 0 | 0 | 0 | 1 | 0 | 0 | 0 | 0 | 1 |
| ARR6 | 0 | 0 | 0 | 0 | 0 | 1 | 0 | 0 | 0 | 0 |
| ARR7 | 0 | 0 | 0 | 0 | 0 | 0 | 1 | 0 | 0 | 0 |
| ARR8 | 0 | 0 | 0 | 0 | 0 | 0 | 0 | 1 | 0 | 0 |
| ARR9 | 0 | 0 | 0 | 0 | 0 | 0 | 0 | 0 | 1 | 0 |

This model supposes that the stator is rigid and the rotor has a contact layer specified as a linear spring with an equivalent rigidity in the axial and tangential direction.

## 4. Electrical equivalent circuit

In Figure 5, $r_L$: is a function of the load torque and applied pre-load pressure. This resistor will model the vibration taking place during the actuation of the motor. It will also take into account of the mechanical and viscous losses in the bearing and other related parts of the ultrasonic motor [5]. Due to the complexity of the interaction between the stator and the rotor, the value of $r_L$ has yet to be established. In our case, it will be derived experimentally to establish their relationship.

The blocking capacitance Cd lowers the power factor. It would have no effect on the motor's efficiency if there were no line resistance connected between the power supply and the motor. However, under actual operating condition, a lower power factor affects the efficiency, owing to the power source's high internal resistance. To improve the power factor, we can place an inductor in parallel to Cd as shown in Figure 6.

If Cd is completely cancelled by the inductor, we can then use the simplified equivalent circuit in Figure 7.

Although one may find the physical significance and relationship of the electrical elements in the equivalent circuit easy to understand, its computational analysis is wearing because the diode is a non-linear element. For the individual phase A and B, the losses and outputs are quantities that vary sinusoidally.

Even though, the phase difference between A and B is 90°, the losses or output power is in fact 180° as they are expressed in terms of the squares of either the current or the voltage. If these quantities are added together, the resultant is a constant. If we separate the equivalent circuit for phases A and B by removing the diode and the inductor, with the resistor representing all mechanical losses, we can treat the circuit as a simple A.C. circuit.

## 5. Model compilation and validation

The series elements are modeled by junction 1 (Equal flow) and those in parallel are modeled by the junction 0 (Equal effort).

After the exhibition of the used graphical model, with bond graph approaches, our task is to implement this model on SYMBOLS; we have implanted the uncoupled bond graph model.

The Figure 10 represents the motor speed without load. The figure 11 shows the evolution of the rotation speed as a function of different loads applied.

Considering the parameter values of the motor used for the simulation (see table 1), the bond graph model developed was simulated, in the steady and transient state of motor. The optimal parameters of the excitation voltages frequency have been tracked and evaluated to 46.65 kHz as frequency, 570 volts as excitation voltage amplitude and $\pi/2$ rad as the shift between the two excitations. The performances of the motor were estimated by applying various loads in the phase of the steady state after 1.5 s of operation. The influence of the application of the loads and consequently the evolution of torque and rotor speed are presented in the following figures. From time 1.5 s, the motor was loaded by load torque of 2 Nm, 3 Nm, 300 Nm. It will be noticed that the speed decreases, when the applied load increases. The figures 12 and 13 show the motor torque characteristics for various loads, which illustrate what happens if a load torque is applied to the rotor after 2 s of operation, the driving torque

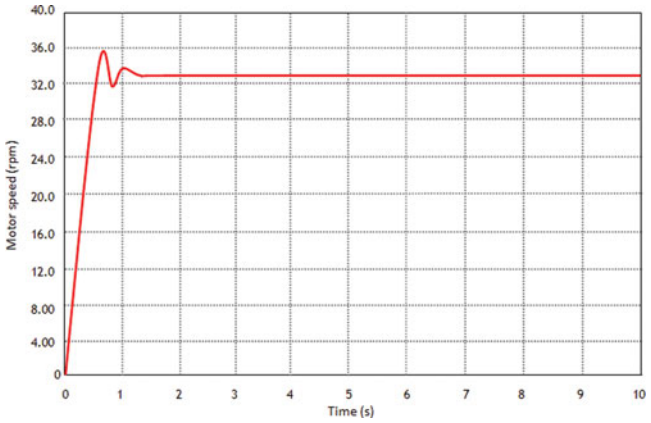


**Figure 10.** The motor speed without load.

provided by the stator has to increase in order to balance the load torque. Therefore, the driving zone widens (the no-slip points move away from the wave crests), whereas the braking zones contract. The rotor velocity is equal to the stator horizontal velocity at the no slip points; therefore, moving no slip points down the velocity profile cause the rotor to slow down.

## 6. Diagnostic of the motor

### *6.1. Linearized bond graph model*

A number of methods have been developed for fault detection and isolation. All methods of fault detection work by designing residual functions. The residual represents the difference between an estimated value and a measured one, which should be zero during normal operation, but large in the presence of faults [24].

In practice, there is a distinction between the detection of fast acting, possibly safety critical faults, and faults which are non-safety-critical and slower to develop, for example due to wear. The former are most likely to be detected by state-estimation and instantaneous comparison of prediction with measurement, while the latter are detected using parameter estimation techniques which require a certain time window and excitation of the system.

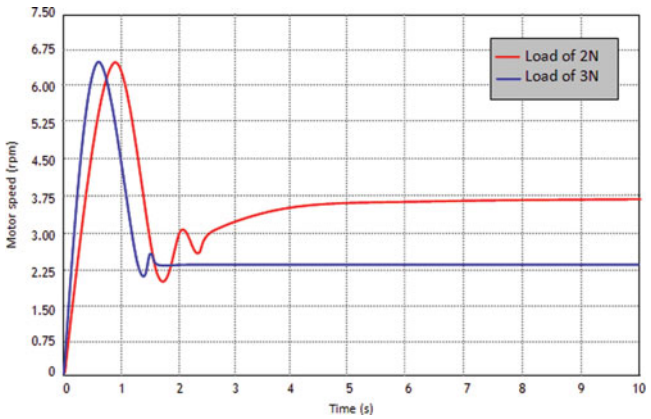


**Figure 11.** Motor speed as a function of time for a load of 2N.

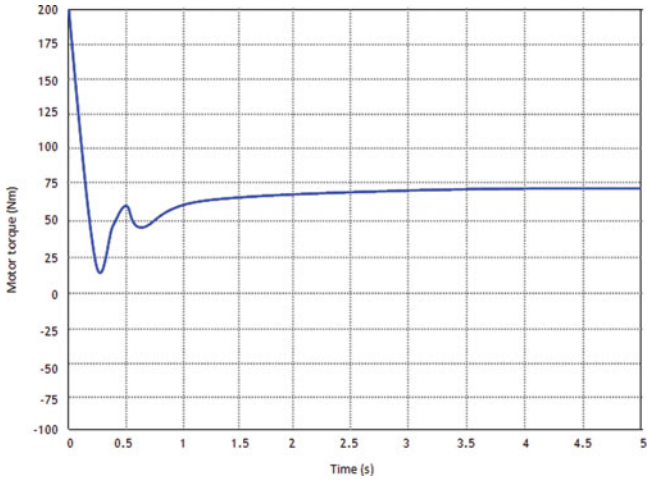


**Figure 12.** Motor speed as a function of time for a load of 3N.

Probability analysis can be used to judge from the residual values, when a fault or change has appeared. This paper is concerned primarily with detection of fast-acting faults, detected via state estimation. Isolation, in the literature, means diagnosis of the faulty component. If faults are allowed to occur simultaneously, then for a diagnosis, at least as many independent residual functions as faults considered are required. In practice, it is usually assumed that only one fault occurs at a time, which facilitates more robust fault diagnosis. The bond graph model of the process is represented by Figure 14.

### *6.2. Generation of the analytical redundancy relations (ARR)*

The ARR are symbolic equations representing constraints between different known process variables (parameters, measurements and sources). They are obtained from the behavioural model of the system through different procedures of elimination of unknown variables. Numeric evaluation of each ARR is called a residual, which is used in model based Fault Detection and Isolation (FDI) algorithm. The quality and efficiency of a diagnosis system

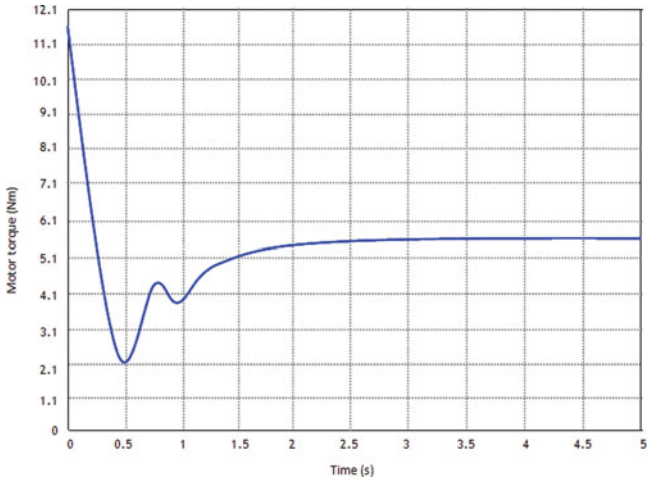


**Figure 13.** Evolution of traction force a function of time for a load of 300N.

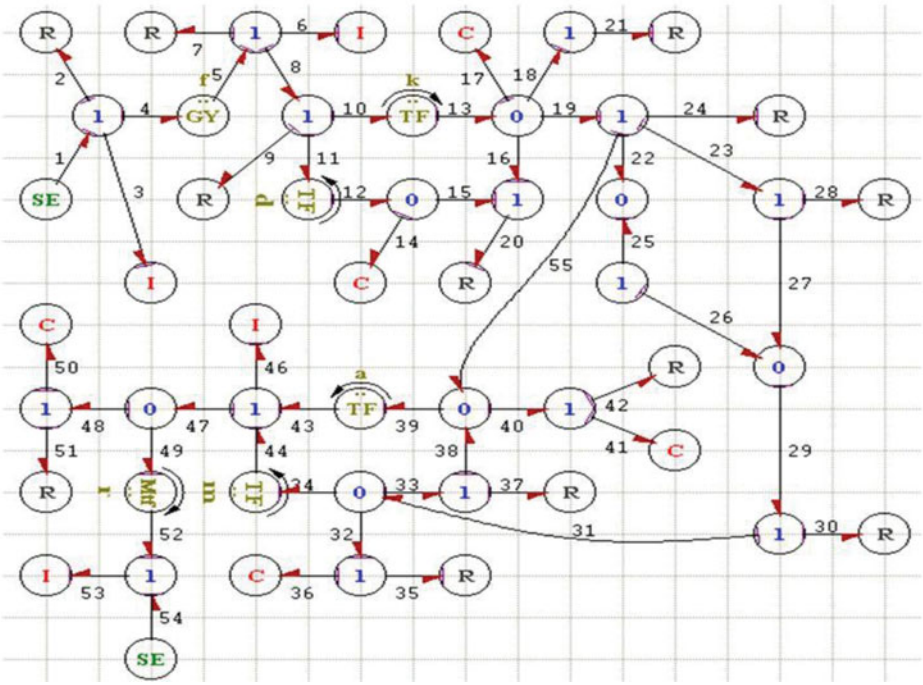


**Figure 14.** Bond graph model of the process.

depends closely on the availability and relevance of the information it can retrieve from the diagnosed plant. The sensors distributed on the system are the source of the fault information.

Previous diagnosis work has been done on the hypothesis of the sensors placed reasonably in advance. In reality, the number or cost of sensors available will be limited and this will, of course, places restrictions on the resolution of data.

As a result, it would be necessary in practice to optimize the number and location of sensors for a given problem. The issue of determining the optimum number of sensors for a particular application, together with their best possible locations, has received considerable attention recently. The goal of these sections is to provide an optimal sensor placement method on the bond graph model in order to make all the components monitored.

Let given a bond graph model obtained from physical process (Figure 14). We suppose that the sensors are not placed yet on the bond graph model. Let xi and yj the binary variables to express the potential sensor placement on the junction nodes such as [24]:

$$x_i = \begin{cases} 1 & \text{if the ith sensor is placed on the ith 0} \\ 0 & \text{otherwise} \end{cases} \tag{4}$$

$$y_j = \begin{cases} 1 & \text{if the ith sensor is placed on the ith 1} \\ 0 & \text{otherwise} \end{cases} \tag{5}$$

N0 number of "0" junctions, N1 number of "1" junctions, ni number of bonds around the ith "0" junction (i = 1, N0), mj number of bonds around the jth "1" junction (j = 1, N1), in the following, "f" and "e" denote flow and effort vector, respectively.

Equations of the ith "0" junction are:

$$\begin{cases} \sum_{k=1}^{ni} a_k f_k = 0 \\ e_k = e_{Ci} \quad \text{where } k = 1, n_i - 1 \end{cases} \qquad a_i = \begin{cases} 1 & \text{if the half-arrow is toward junction} \\ 0 & \text{otherwise} \end{cases} \tag{6}$$

Equations of the jth "1" junction are:

$$\begin{cases} \sum_{l=1}^{mj} a_l f_l = 0 \\ f_l = f_{Rj} \quad \text{where } k = 1, m_j - 1 \end{cases} \qquad a_l = \begin{cases} 1 & \text{if the half-arrow is toward junction} \\ 0 & \text{otherwise} \end{cases} \tag{7}$$

The known variables are represented in the bond graph by the measured variables given by effort (De) and flow (Df) detectors, and the input variables which can be a constant source of effort and flow Se, Sf or a modulated source of effort and flow MSe, MSf. K is the set of known variables.

$$K = \text{MSe} \cup \text{MSf} \cup \text{De} \cup \text{Df} \cup \text{u} \tag{8}$$

X is the set of the unknown variables represented by the power variables (flow and effort).

$$\text{X(t)} = \{e_1(t), f_1(t)\} \cup \{e_2(t), f_2(t)\} \ldots \{e_n(t), f_n(t)\} \tag{9}$$

where n is the number of bond graph R, C and I elements. The set of constraints can be decomposed into four sub sets according to the bond graph methodology.

- The behavioural constraints: gather the sets of algebraic and differential constraints, and describe the physical phenomena on the bond graph elements.
- The structural constraints: those constraints are independent from the metric notions and represent the laws of power and matter conservation on the system and are deduced from the junctions 0 and 1 on the bond graph model.
- The measurement constraints: describe the available measurement on the system. They express the manner the sensors transform some state variables of the process into output signals which can be used for system control and diagnosis. The sensor output represents the power variable common for all the inputs and outputs of the junction.
- The differentiation constraints: those constraints are not directly related to the physical system, thus they do not appear explicitly on the bond graph model. They are used to calculate the derivative of the known efforts and flows.

Based on causal properties of the bond graph modeling, the unknown variables can be calculated using covering causal paths. For the "0" and the "1" junction the unknown variables based on fixed causality are calculated as follows:

$$\begin{cases} f_{C_i} = \phi_{C_i}\left[S\{(1 - x_i)(e_{Ci}) + x_i De_i\}\right] \\ e_{C_i} = \frac{1}{S}(1 - x_i)\phi_{C_i}^{-1}(f_{Ci}) + x_i De_i \end{cases} \quad \text{avec i} = 1.\text{N} \tag{10}$$

$$\begin{cases} e_{R_j} = \phi_{R_j}\left[(1 - y_j)(f_{Rj}) + y_j Df_j\right] \\ f_{R_j} = (1 - y_j)\phi_{R_j}(e_{Rj}) + y_j Df_j \end{cases} \quad \text{avec j} = 1.\text{N}_1 \tag{11}$$

$$\begin{cases} e_{L_k} = \phi_{L_k}\left[(1 - z_k)(f_{L_k}) + z_k Df_k\right] \\ f_{L_k} = (1 - z_k)\phi_{L_k}(e_{L_k}) + z_k Df_k \end{cases} \quad \text{avec k} = 1.\text{N}_1 \tag{12}$$

The residuals are designed to be sensitive to a fault that comes from a specific sensor and as insensitive as possible to all the others sensor faults. This residual will permit us to treat not only with single faults but also with multiple and simultaneous faults. The input-output

relationship of the system after being incorporated with a normal operation model can be described approximately as follows:

$$K = F(X) \tag{13}$$

X is the fault vector with each input xi representing a measure of the fault level for fault (x1: fault in De1, x2: fault in De2, …). K is the state variable residual vector, with each input representing a particular state-variable residual. F(X) is a nonlinear function defining the relationship between different faults at different levels and the state variable residuals k.

Fault diagnosis, which entails the determination of the kind and location of the detected fault from a list of possibilities, needs to use the resulting K (known) to find the causes X (unknown).

The nonlinear Equation (1) cannot get unique solutions for X for a given K if $m < n$ and may result in inconsistencies $n < m$, but it would not lose any generality to assume m = n. If F(x) is known, multiple simultaneous fault diagnosis becomes easy. However, it is very difficult, if not impossible, to find F(x). To simplify equation (1), the first two items of McLaren's series can be used to linearize the nonlinear equation. Fault detection (FD) is a process of binary decision. This is an estimate positive or negative for the presence of a fault. This response is given by a decision criterion generally defined in an algorithm. The state detection, binary result of the detection process can be written in general as follows:

$$FD = \begin{cases} 1 \text{ if the criteria of decision is validated} \\ 0 \text{ otherwise} \end{cases} \tag{14}$$

The state of detection depends on one or more parameters. These parameters should then be adjusted according to measurement conditions, possibly as properties of the target roughness or defects sought. Two cases for the actual presence of a fault (PF) are possible:

$$PF = \begin{cases} 0 \text{ if the signal does not correspond to a fault} \\ 1 \text{ if the signal corresponds to a fault} \end{cases} \tag{15}$$

Depending on the value of the state detection (det), four combinations are possible. Both errors are possible: error detection and false alarm. False alarm is the erroneous detection of a fault. It may lead to the substitution of a piece yet intact, constituting an undue cost to the manufacturing process or revision of the device. We propose the application of simple thresholding algorithm. It gives a positive response to detection if, for at least one measuring point ($n_i$, $n_j$), the value s($n_i$, $n_j$) the modulus of the signal is greater than the detection threshold $\theta$ fixed either.

$$\det(DC) = \begin{cases} 1 \quad \text{if} \exists (n_i, n_j), \left| s(n_i, n_j) \right| \geq DC \\ 0 \quad \text{otherwise} \end{cases} \tag{16}$$

DC is an adjustment of the decision criterion. It can be set for each set of measurement conditions, while remaining the same for all assessments conducted under the same conditions. For our application DC = 0.11 unit. It may be possible to adjust the detection threshold based on the fault. The amplitude of the signal depends on the fault size. It is possible to consider that small faults are not harmful to the system. Its threshold value depends on the measurement conditions and the minimum fault size. The algorithm developed in this section estimates the detection state det = 0 or det = 1 from any figure corresponding to a PF = 0 or PF = 1. This algorithm relies on a detection threshold DC whose value must be determined for each set of measurement conditions. The optimal threshold value is chosen by covering all possible threshold values and calculating their statistically representative set of images. Sensitivity is

the number of correct detections measured $n_{CD}$ divided by the total number of correct detections possible on a statistically sufficient number of samples, or

$$Se = \frac{n_{CD}}{n_{CD} + n_{SD}} = \frac{n_{CD}}{n_{PF_1}} PF_1 = PF \text{ (if the signal corresponds to a fault)} \quad (17)$$

The sensitivity is thus equal to the rate of correct detection and quantifies the ability of the detection process to respond correctly when the PF is 1. The specificity is the number of non-correct detections measured divided by the total number of non-correct detections possible.

$$S_p = \frac{n_{NCD}}{n_{NCD} + n_C} = \frac{n_{NCD}}{n_{PF_0}}, PF_0 = PF \text{ (if the signal does not correspond to a fault)} \quad (18)$$

Precision is the total number of states detection consistent with the hypothesis assessed divided by the total number of samples as follows:

$$P_r = \frac{n_{CD} + n_{NCD}}{n_{PF_0} + n_{PF_1}} \quad (19)$$

For our application, the equations in junctions are given by:
For 1i junction:

$$\begin{cases} f_3 = f_1, f_3 = f_2 \\ e_1 - e_2 - e_3 - e_4 = 0 \\ e_{I_1} = \varphi_{I_1}\left[\left(1 - y_1\right) f_3 + y_1 Df_1\right] \\ f_{I_1} = \left(1 - y_1\right) \varphi_{I_1}(e_3) + y_1 Df_1 \end{cases} \quad (20)$$

For 0j junction:

$$\begin{cases} e_{14} = e_{12}, e_{14} = e_{15} \\ f_{12} - f_{14} - f_{15} = 0 \\ f_{C_1} = \varphi_{C_1}[S\{(1 - x_1) e_{14} + x_1 De_1\}] \\ e_{C_1} = \frac{1}{S}(1 - x_1) \varphi_{C_1}^{-1} f_{14} + x_1 De_1 \end{cases} \quad (21)$$

From equations of junctions we generate the following ARR:

$$ARR_1 : Se_1 - \overset{*}{De}_1 - \varphi_{I_1}\left[\left(1 - y_1\right) f_3 + y_1 Df_1\right] - \overset{*}{De}_2 = 0$$
$$ARR_2 : f(1 - y_1)\Phi_{I_1}(e_3)_1 + \Phi_{I_1}[(1 - y_2) f_6 + y_2 Df_2] - \overset{*}{De}_3 - \overset{*}{De}_4 + y_1 Df = 0$$
$$ARR_3 : \tfrac{1}{S}(1 - x_1)\, \Phi_{C_1}^{-1}(f_{14}) + \tfrac{1}{S}(1 - x_2)\, \Phi_{C_2}^{-1}(f_{17}) + x_2 De_2 - \Phi_{R_4}[(1 - y_3) f_{20} + y_3 Df_3] + x_1 De_1 = 0$$
$$ARR_4 : -\Phi_{R_5}[(1 - y_4) f_{21} + y_4 Df_4] + \tfrac{1}{S}(1 - x_2)\, \varphi_{C_2}^{-1}(f_{17}) + x_2 De_2 = 0$$
$$ARR_5 : x_2 De_2 - \Phi_{R_6}[(1 - y_5) f_{24} + y_5 Df_5] - \overset{*}{De}_5 + \tfrac{1}{S}(1 - x_2)\, \varphi_C^{-1}(f_{17}) + = 0$$
$$ARR_6 : \overset{*}{De}_7 - \varphi_{r_2}\left[\left(1 - y_6\right) f_{35} + y_6 Df_6\right] - \overset{*}{De}_8 = 0$$
$$ARR_7 : \tfrac{1}{m}\overset{*}{De}_7 + Se_{45} - \Phi_{I_3}[(1 - y_7) f_{46} + y_7 Df_7] - \overset{*}{De}_{10} + De_9 = 0$$
$$ARR_8 : \overset{*}{De}_{11} - \varphi_{I_4}\left[\left(1 - y_8\right) f_{53} + y_8 Df_8\right] + Se_{54} = 0$$
$$ARR_9 : \overset{*}{Df}_2 - y_3 Df_3 - \Phi_{C_1}[S\{(1 - x_1) e_{14} + x_1 De_1\}] - (1 - y_3)\Phi_{R_4}(e_{20}) = 0$$
$$ARR_{10} : \overset{*}{Df}_1 - \Phi_{C_2}[\{S(1 - x_2) e_{17} + x_2 De_2\}] - y_3 Df_3 - (1 - y_4)\Phi_{R_5}(e_{21}) - y_4 Df_4 - (1 - y_3)\Phi_{R_4}(e_{20}) = 0$$

### 6.3. Faults signature table

From the binary variables xi and yj we can determine the final structure of the monitored system [2]. Two 10-sensor placement combinations provide the monitorability of the all components.

The fault signatures are not different from each other (I1 and I2) and not equal to zero, then the components I1 and I2 are not monitored but R4, R5, R6, r2, I3, I4, C1 and C2 are monitored.

The fault signatures are different from each other and not equal to zero, then the components I1, I2, R4, R5, R6, r2, I3, I4, C1 and C2 are monitored. For the faults detection of ultrasonic linear motor we use the precedent Analytical Redundancy Relations. We create the faults on monitoring components with this software fault here is considered in the total absence or the deviation of the nominal value given out by the component to monitor.

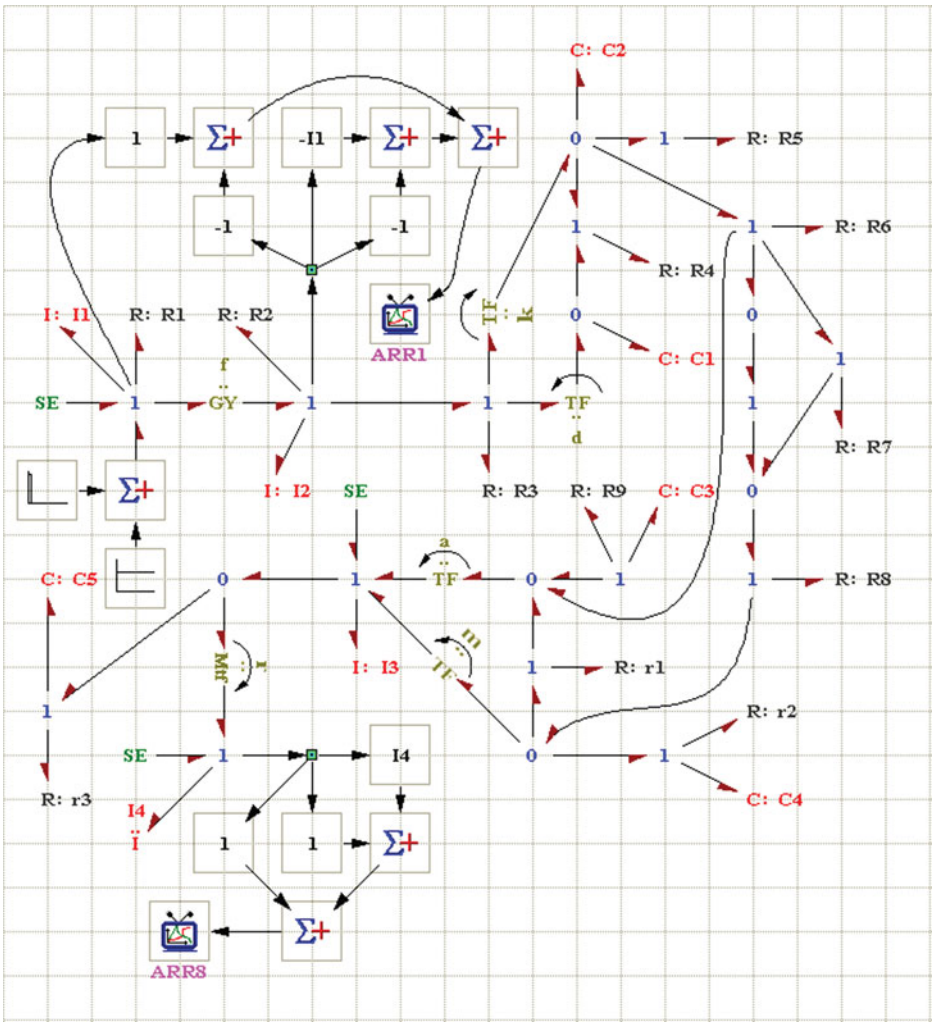


**Figure 15.** Bloc diagram.

### 6.4. Sensitivity of the detector $Df_1$ from the faults on the inertia $I_1$ and the resistance $R_1$

In the first time, we create a fault between the instant t = 2 and t = 2.5 s. The bloc diagram of the process is illustrated by (figure 16):

The failures on I1 and R1 are characterized by the presence of the detector Df1 in the analytical redundancy relation ARR1. We note that the residual ARR1 is sensitive to the failures which affect I1 and R1, but residuals ARR2, ARR3, ARR4, ARR5, ARR6, ARR7, ARR8 and ARR9 are equals to zero.

### 6.5. Sensitivity of the detector $Df_2$ from the faults of the inertia $I_2$ and the resistance $R_2$

By the same procedure we can monitored the components I2 and R2

The generated ARRs reaction is very fast see Figure 15. The deviation of the relations ARR1, ARR4, ARR5, ARR6, ARR7, ARR8 and ARR9 in this time is normal (constant values). We see that residuals ARR2 is sensitive (seen the presence of Df2 in this relation).

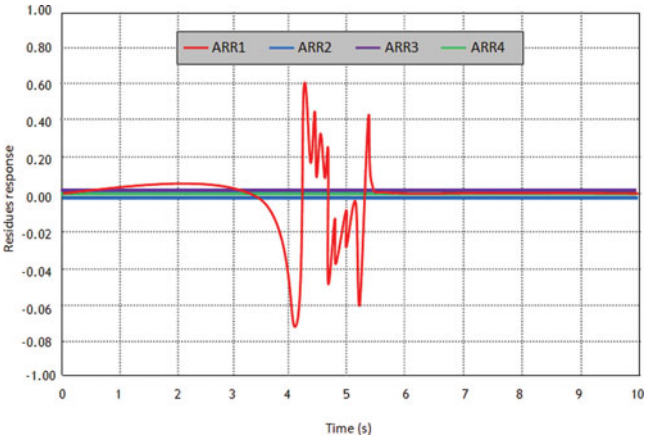


**Figure 16.** Sensitivity of detector $Df_1$.

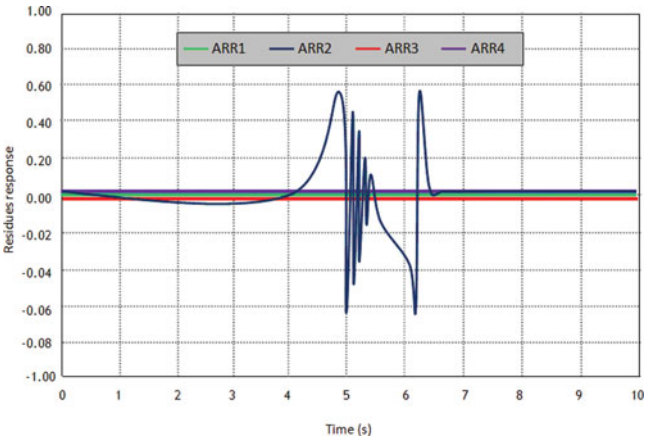


**Figure 17.** Sensitivity of detector $Df_2$.

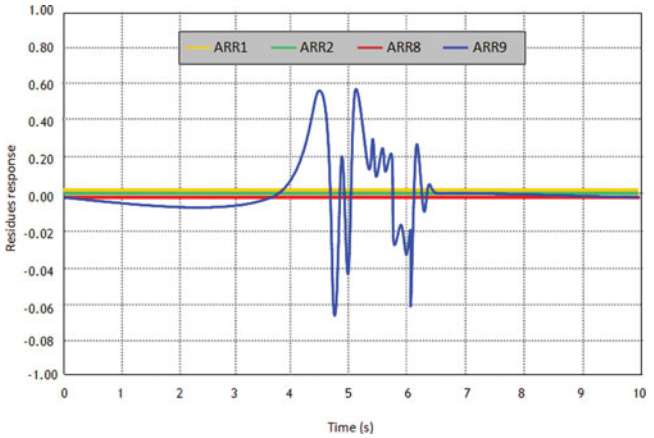


**Figure 18.** Sensitivity of detector $De_1$.

### *6.6. Sensitivity of the detector $De_1$ from the fault of the capacity C1*

The deviation of the relations ARR1, ARR2, ARR3, ARR4, ARR5, ARR6, ARR7 and ARR8 in this time is normal (constant value). We see that residual ARR9 are sensitive (seen the presence of De1 in this relation).

## Conclusions

This work has presented piezomotor and more precisely, travelling wave ultrasonic annular motor. Its advantages and drawback have been explained. Piezomotors have specificities that are very interesting if they match application's needs: high torque/low speed, holding torque, silent operation, reactivity, high integration level. Because of the ultrasonic linear motor's complexity, precise analysis using analytic method is very difficult. Nevertheless, this modeling methodology has been presented in order to show that it is possible to model ultrasonic motors analytically. In the same way, the method of Bond Graph could be applied. Bond Graph is an explicit graphical tool for capturing the common energy structure of systems. In the vector form, it gives a concise description of complex systems. By this approach, a physical system can be represented by symbols and lines, identifying the power flow paths. The method used illustrates the process principle working. We have using the structural junction equations for generating the analytical redundancy relations like failures indicators. The bond graph tool is the unified modeling method and it facilitates the functional and structural analysis of the complex systems. The multi-energy bond graph based approach used here for fault detection of the complex systems will be in perspective following by fault isolation and identification of eventual failure.

The bond graph tool and software Symbols are proven powerful and convenient means for this project which included the modelling, the monitoring, the simulation and the analysis of the results. The results found here are proven interesting because the simulation of defects in quite precise moments were confirmed by the software of simulation starting from the sensitivity of the indicators installed.

The main contribution of the work presented in this paper consists in the description of Bond Graph modeling of traveling wave ultrasonic motor, and simulation characteristics. The modeling of the traveling wave ultrasonic motor and its simulation is an important task to

understand the principle of operation and its dynamic behavior. The generation of the analytical redundancy relations by the Bond Graph approach shows some interesting characteristics: They are simple to include/understand, since they correspond to relations and variables which are posted by the model Bond Graph image of the physical process, these relations are deduced directly from the graphic presentation. They can be generated in symbolic form system and thus adapted to a data-processing implementation.

## References


[1] Watson, B., Friend, J., & Yeo, L. (2009). *Sensors and Actuators A*, *152*, 219–233.
[2] Hanly, E.J., & Talamini, M.A. (2004). *The American Journal of Surgery*, *188*, 19S–26S.
[3] Menciassi, A., Quirini, M., & Dario, P. (2007). *Minimally Invasive Therapy and Allied Technologies*, *16*, 91–100.
[4] Elka, E., Elata, D. & Abramovich, H. (2004). *Journal of Micro Electromechanical Systems*, *13*, 2, 332–341.
[5] Khemliche, M., Badoud, A. & Latreche, S. (2010). *Leonardo Journal of Sciences*, 16.
[6] Low, T. S. & Guo, W. (1995). *Journal of Micro Electromechanical Systems*, *4*, 4, 230–237.
[7] Coté, F., Masson, P., Mrad, N. & Cotoni, V. (2004). *Composite Structures*, *65*, 471–484.
[8] Dong, X. & Meng, G. (2006). *International Journal of Advanced Manufacturing Technology*, *27*, 841–844.
[9] Devoe, D. L. & Pisano, A. P. (1997). *Journal of Micro-electromechanical Systems*, *6*, 3, 266–270.
[10] Hagood, I. & McFarland, A. J. (1995). *IEEE Transactions on Ultrasonics, Ferroelectrics and Frequency Control*, *42*, 2, 210–224.
[11] Goldfarb, M. & Celanovic, N. (1997). *IEEE Control Systems Magazine*, *17*, 3, 69–79.
[12] Adrians, T. S., De Koning, W. L. & Banning, R. (2000). *IEEE/ASME Transactions on Mechatronics*, *5*, 4, 331–341.
[13] Samantaray, A.K., Medjaher, K., Ould Bouamama, B., Staroswiecki, M., & Dauphin-Tanguy, G. (2005). *Simulation Modeling Practice and Theory Journal*, 237–262.
[14] Paynter, H. M. (1961). *Analysis and design of engineering systems*, MIT Press, Cambridge, MA.
[15] Ould Bouamama, B., Busson, F., Dauphin-Tanguy, G., & Staroswiecki, M. (2000). Analysis of structural properties of thermodynamic bond graph models. In Proceeding of the 4th IFAC: Fault Detection Supervision and Safety for Technical Processes, vol. 2 IFAC, Budapest, Hungary, pp. 1068–1073.
[16] Zitouni, N., Khiari, B., Andoulsi, R., Sellami, A., Mami, A. & Hssen, A. (2011). *IJCSNS International Journal of Computer Science and Network Security, 11, 6*, 105–114.
[17] Thoma, J. (1975). *Introduction to Bond Graphs and Their Applications*, Pergamon Press, Oxford.
[18] Karnopp, D., & Rosenberg, R. (1974). *System Dynamics: A Unified Approach*, John Wiley, New York.
[19] Karnopp, D. C., Margolis, D. L., & Rosenberg, R. C. (2006). *System dynamics modeling and simulation of mechatronics systems*, John Wiley & Sons, New Jersey.
[20] Fernandez, J. & Perriard, Y. (2003). ComparativeAnalysis andModeling of Both Standing and Traveling Wave Ultrasonic LinearMotor, in Proceedings of the IEEE International Ultrasonics Symposium, Honolulu, Hawaii, USA, October, vol. 2, 1770–1773.
[21] Fernandez, J., Ruffieux, Y. & Perriard, Y. (2005). Design Optimization Analysis of a Standing Wave Ultrasonic Linear Actuator, in Proceedings of the IEEE International Ultrasonics, Ferroelectrics, and Frequency Control Conference, Rotterdam, The Netherlands, September, vol. 1, 311–314.
[22] Shuichi, K., Hiroshi, Y., Daisuke, K., & Kentaro, N. (2010). *Physics Procedia*, *3*, 1, 1053–1058.
[23] Helin, P., Sadaune V., Druon C., & Tritch J. B. (1998). *IEEE/ASME Transactions on Mechatronics*, *3*,(1), 3–8.
[24] Khemliche, M., Ould Bouamama, B. & Haffaf, H. (2006). *Sensors and Actuators Journal, Elsevier*, *4*, 92–98.